Energy Policy 38 (2010) 4400–4410

Contents lists available at ScienceDirect

Energy Policy

journal homepage: www.elsevier.com/locate/enpol

The variability of interconnected wind plants

Warren Katzenstein*, Emily Fertig, Jay Apt

Carnegie Mellon Electricity Industry Center, Department of Engineering & Public Policy and Tepper School of Business, Carnegie Mellon University, 5000 Forbes Avenue, Pittsburgh, PA 15213, USA

ARTICLE INFO

Article history:
Received 8 January 2010
Accepted 25 March 2010
Available online 18 April 2010

Keywords:
Wind power
Wind variability
Interconnected wind plants

ABSTRACT

We present the first frequency-dependent analyses of the geographic smoothing of wind power's variability, analyzing the interconnected measured output of 20 wind plants in Texas. Reductions in variability occur at frequencies corresponding to times shorter than ~24 h and are quantified by measuring the departure from a Kolmogorov spectrum. At a frequency of 2.8×10^{-4} Hz (corresponding to 1 h), an 87% reduction of the variability of a single wind plant is obtained by interconnecting 4 wind plants. Interconnecting the remaining 16 wind plants produces only an additional 8% reduction. We use step change analyses and correlation coefficients to compare our results with previous studies, finding that wind power ramps up faster than it ramps down for each of the step change intervals analyzed and that correlation between the power output of wind plants 200 km away is half that of co-located wind plants. To examine variability at very low frequencies, we estimate yearly wind energy production in the Great Plains region of the United States from automated wind observations at airports covering 36 years. The estimated wind power has significant inter-annual variability and the severity of wind drought years is estimated to be about half that observed nationally for hydroelectric power.

© 2010 Elsevier Ltd. All rights reserved.

1. Introduction

Currently 29 of the United States of America have renewables portfolio standards (RPS) that mandate increasing their percentage of renewable energy, and the lower chamber of the United States Congress has enacted a federal renewable electricity standard (Database of State Incentives for Renewables and Efficiency, DSIRE, 2009; Waxman and Markey, 2009). Major electricity markets such as California, New York, and Texas expect wind to play a large role in meeting their RPS. As a result of the state RPS requirements and a federal production tax credit equivalent to a carbon dioxide price of approximately $20/metric ton (Dobesova et al., 2005), wind power net generation is currently experiencing very high growth rates (51% in 2008, 28% average annual growth rate over the past decade) in the United States (EIA, 2009).

Wind power's variability and fast growth rate have led areas including Cal-ISO, PJM, NY-ISO, MISO, and Bonneville power to undertake wind integration studies to analyze if their systems can accommodate significant (5–20%) penetrations of wind power (CAISO, 2007; DOE, 2008; EnerNex, 2006; GE, 2008; Hirst, 2002). Included in each integration study is how wind power variability can be mitigated with options such as storage, demand response, or fast-ramping gas plants. Some system operators are beginning to charge wind operators for costs arising from the integration of high wind penetration in their system. In 2009, the Bonneville Power Authority (BPA) introduced a wind integration charge of $1.29 per kW per month (~0.6¢/kWh assuming a 30% capacity factor), citing reliability risks and substantial costs encountered in fulfilling 7% of their energy needs with wind power (BPA, 2009).

Previous studies have shown that interconnecting wind plants with transmission lines reduces the variability of their summed output power as the number of installed wind plants and the distance between wind plants increases (Archer and Jacobson, 2007; Czisch and Ernst, 2001; Giebel, 2000; IEA, 2005; Kahn, 1979; Milligan and Porter, 2005; Wan, 2001). Kahn (1979) estimates the increased reliability of spatially separated wind plants, writing that "wind generators can displace conventional capacity with the reliability that has been traditional in power systems." Kahn (1979) calculates the loss of load probability (LOLP) and the effective load carrying capability (ELCC) of up to 13 interconnected California wind plants.

Czisch and Ernst (2001) and Giebel (2000), in separate studies, show the correlation between wind plants decreases with distance. Each concludes wind power variability is reduced by summing the output power from spatially separated wind plants. Czisch and Ernst (2001) and Giebel (2000) both find that wind plant outputs are correlated even over great distances (correlation coefficient > 0).

Milborrow (2001) shows a smoothing effect by calculating the output power change over a certain time interval (step change) of wind plants. He finds the 1-h power swing of 1860 MW of wind

* Corresponding author. Tel.: +1 412 390 6550; fax: +1 412 268 3757.
E-mail address: warren@cmu.edu (W. Katzenstein).

0301-4215/$ - see front matter © 2010 Elsevier Ltd. All rights reserved.
doi:10.1016/j.enpol.2010.03.069

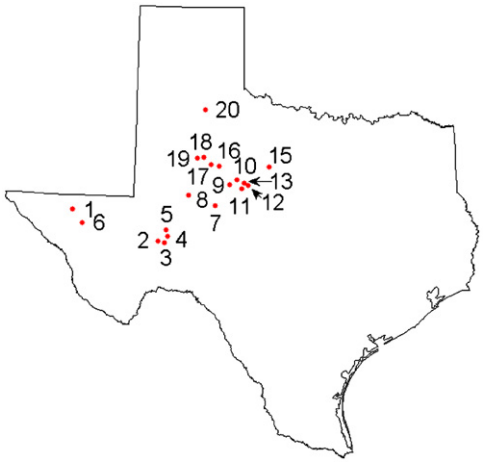

Fig. 1. Locations of the ERCOT wind plants from which data were obtained.

power in Western Denmark over a 3-month period in 2001 was at most 18% of installed capacity compared with 100% for a single wind plant. In contrast, Bonneville Power Authority in the US Pacific Northwest experienced a maximum 1-h step change of 63% in 2008 for their 1670 MW of wind power.

Archer and Jacobson, (2007) wrote that interconnected wind plants would produce "steady deliverable power." They use hourly and daily averaged wind speed measurements taken at 19 airports located in Texas, New Mexico, Oklahoma, and Kansas to estimate generation duration curves and operational statistics of wind power arrays. They found that "an average of 33% and a maximum of 47% of yearly averaged wind power from interconnected farms can be used as reliable, baseload electric power" (Archer and Jacobson, 2007).

The previous studies analyze wind's variability primarily in the time domain, using metrics such as 10-min step change histograms, correlation coefficients, and LOLP.

Frequency domain analysis is a powerful complementary method that can be used to characterize variability and evaluate whether and at what frequencies smoothing occurs as more wind plants are introduced into a system. We use Fourier transform techniques to estimate the power spectral density (PSD) (Apt, 2007; Cha and Molinder, 2006; Press et al., 1992) and characterize the variability of actual wind plants within ERCOT, the electricity market serving most of Texas. We also use step change analyses and correlation coefficients to characterize the variability of ERCOT wind plants and wind plants modeled from wind monitoring stations located throughout the Midwest and Great Plains and compare our results with previous studies.

To characterize the year-to-year variations of wind power production, we calculate the yearly output of wind power by modeling wind plants over a span of 36 years. We examine the existence and likely severity of wind drought years as compared to hydroelectric power reduction by rainfall droughts.

2. Data

We use both ERCOT wind plant power output data and National Oceanic and Atmospheric Administration (NOAA) wind speed data for our analyses. We use 15-min time resolution real power output data from 20 wind plants within ERCOT (Fig. 1).[1] The ERCOT data were obtained from ERCOT's website. Data sets from three wind farms with over ten days of consecutive zeros were discarded. There were minor data dropouts in data from the remaining 20 wind farms, but the correlation coefficients were insensitive to exclusions of data dropout periods, so the correlations displayed include all data. If necessary, data from each wind plant are scaled to the end-of-the-year capacity of the wind plant to adjust for mid-year capacity additions. We use 2008 wind power data from Bonneville Power Authority to analyze if results similar to our ERCOT results are seen in another system. BPA provides 5-min system wind power data on its website.[2] There was 0.04% of the data missing from BPA's 2008 wind data set.

When examined in the frequency domain, ERCOT's data exhibit the Kolmogorov spectrum of wind plants as found by Apt (2007). The Nyquist frequency, the highest frequency the data can represent without aliasing, is 5.6×10^{-4} Hz (corresponding to 30 min) for ERCOT's 15-min wind power output data.

We use NOAA ASOS 2-min resolution wind speed data to estimate the effect of interconnecting up to 40 wind plants throughout 7 states located in the Midwest, Southwest, and Great Plains regions[3]. ASOS is a joint project among NOAA, the Department of Defense, the Federal Aviation Administration, and the US Navy with ~1000 stations that automatically record surface weather conditions (NOAA et al., 1998). We selected 40 stations to represent the high wind energy locations of the Great Plains region where wind plants are currently being developed, Archer and Jacobson (2007) analyzed a subset of this region. Each minute, ASOS stations record wind speed and direction averaged over the previous 2 min to the neared nautical mile per hour. Table A1 in the Appendix lists the 40 ASOS sites we used and Fig. 2 plots their location. The average distance between the 40 ASOS sites we use is 785 km and the median distance is 725 km.

There are three limitations to using ASOS wind speed data to model wind plants. The first is that the data are reported as integer knots (NOAA et al., 1998). The second is that the data are a running 2-min average. Both the rounding and averaging reduce the high frequencies we can resolve in the frequency domain (Over and D'Odorico, 2002). A noise floor is evident in the power spectral density, caused by the 1 knot amplitude resolution of the data. The effect of averaging is a departure from the Kolmogorov spectrum at frequencies greater than approximately 2×10^{-4} Hz (periods of 90 min or shorter) that we do not observe in non-ASOS anemometer data. The third limitation of the ASOS data set is prevalence of bad data. In 2007, our selected ASOS sites had an average bad data rate of 7.7%. Spencer Municipal Airport, Iowa (KSPW) had the best data collection in our sample with a bad data rate of 4.6% and Theodore Roosevelt Regional Airport in Dickinson North Dakota (KDIK) had the worst with a bad data rate of 16.5%.

We use NOAA hourly data obtained from airport sites (red squares in Fig. 2) to study how the energy output of wind plants varies over many years. There is significant variation in the historical hourly data sets of the 40 airports prior to ASOS deployment in the 1990s. Some airports recorded wind speeds every third hour and only during the day. Data dropouts of months to years are present in the majority of the data sets. We used only the 16 airports out of the 40 that had hourly wind speed data from 1973 to 2008 and did not have a data dropout greater

[1] Electric Reliability Council of Texas (2009) Entity-Specific Resource Output. Retrieved on 18 Feb. 2009 from ERCOT's Planning and Market Reports. Available at http://www.ercot.com/gridinfo/sysplan/.

[2] Bonneville Power Authority wind generation in balancing authority. Retrieved May 6, 2009. Available at http://www.transmission.bpa.gov/business/operations/wind/.

[3] See Table A1 in the Appendix for a list of specific sites. Data are available at ftp://ftp.ncdc.noaa.gov/pub/data/asos-onemin/.

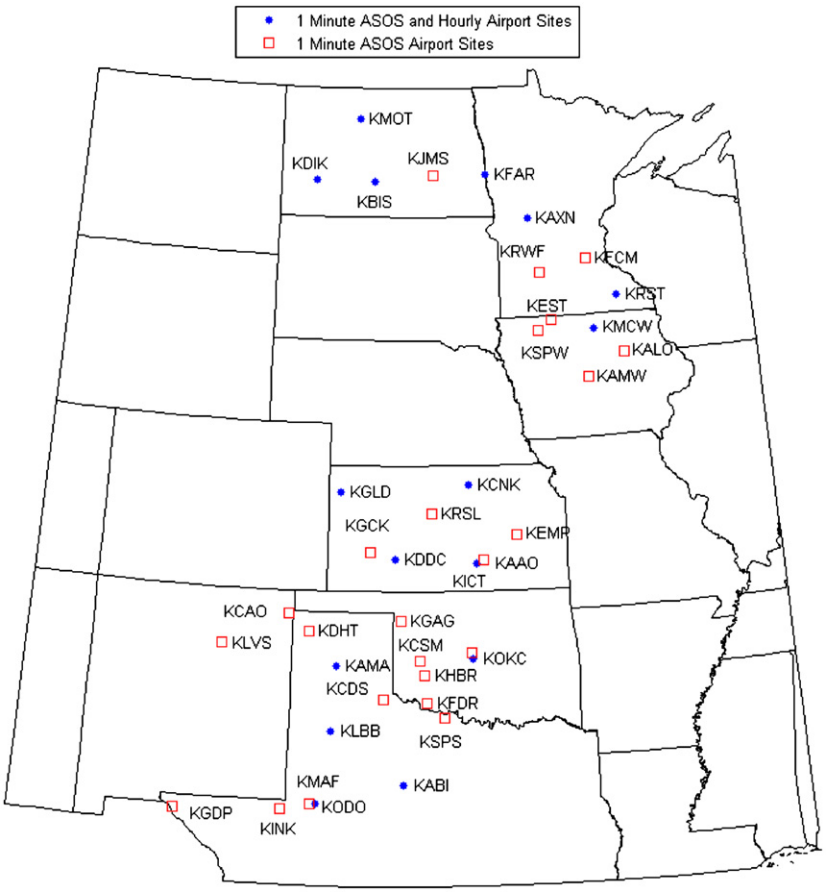

Fig. 2. Locations of the airports from which data were obtained.

than 5 days. The 16 sites are listed in Table A2 in the Appendix and had an average missing data rate of 13%.

3. Methods

3.1. Interconnecting wind plants

We simulate wind plants interconnected with uncongested transmission capacity (sometimes called the copper plate assumption) by summing together either ERCOT wind plant power output data or NOAA airport wind speed data (taken at 8 or 10 m, depending on the station) scaled up to 80 m and transformed to power with a cubic curve (Eq. (1)) that provides a good match to observed data from 1.5 MW turbines and turbine-mounted anemometer data.

$$P(t)=\begin{cases} 341-277v_{wind}+62v_{wind}^2-2.5v_{wind}^3 & \text{if } v_{wind}\geq 2.9\,m/s \text{ and } v_{wind}<14\,m/s \\ 1500 & \text{if } v_{wind}\geq 14\,m/s \\ 0 & \text{if } v_{wind}<2.9\,m/s \end{cases} \quad (1)$$

Previous work indicates that wind power variability can be reduced by either increasing the number of wind plants or increasing the distance between wind plants. For our step change and frequency analyses, we add stations together according to their location. We select an ERCOT wind plant as the starting point, calculate the distance to each of the other stations using a WGS-84 ellipsoidal Earth, and sort the results from closest to farthest wind plant (Vincenty, 1975). We simulate interconnected wind plants by adding the closest wind plant's power to the system, perform step change and PSD analyses, and repeat until all wind plants have been interconnected. The same method is used to add ASOS stations together by distance.

3.2. Missing data

The 1-min ASOS and hourly NOAA data sets are incomplete. For the ASOS data, we treat missing data as follows. If the length of the missing data segment is less than 3 min, then the missing data is filled in by interpolating between the 2 closest points. Any missing data segments longer than 3 min are excluded from the summed result.

For the NOAA hourly data set used for the wind drought analysis, any missing data segments with a length of 3 h or less are filled in by interpolating between the 2 closest points. Any missing data segments with a length greater than 3 h but less than 120 h are filled in using average wind speeds calculated from the previous four weeks for each hour of the day. We then take the time of day average segment that coincides with the missing data segment and scale it to match its boundaries with the boundaries of the surrounding good data segments. Any data set that has a missing data segment longer than 120 h is excluded.

3.3. Scaling wind data to hub height

The airport wind speed measurements were taken at heights of 8–10 m and are scaled up to 80 m before being transformed to power data. We use a logarithmic velocity profile to estimate wind speeds at a hub height of 80 m (Eq. (2); Seinfeld and Pandis,

2006). The logarithmic velocity profile assumes the surface layer is adiabatic. The logarithmic velocity profile depends on a surface roughness length that characterizes the boundary layer near the ASOS station; we use $z_0 = 0.03$ m.

$$u_*(80\,\mathrm{m}) = \frac{u_*}{\kappa}\ln\frac{80}{z_0} \tag{2}$$

where

$$u_* = \frac{\kappa u_*(h_r)}{\ln\frac{h_r}{z_0}}$$

h_r is the reference height, z_0 the surface roughness length, and $\kappa \sim 0.4$ (von Karman constant).

3.4. Correlation analysis

Correlation between power output time series of two wind plants can be quantified by Pearson's correlation coefficient:

$$\rho = \frac{\sum_i (x_i - x)(y_i - y)}{\sigma_x \sigma_y \sqrt{\sum_i (x_i - x)^2}\sqrt{\sum_i (y_i - y)^2}}; (-1 \le \rho \le 1) \tag{3}$$

Power outputs of two wind plants that rise and fall in relative unison have ρ near one, and little smoothing takes place. A correlation coefficient near zero indicates that wind power outputs vary independently of each other. A negative correlation coefficient, although not seen in the data, would indicate anti-correlation between wind power outputs such that high power output from one wind plant is associated with low power output from the other; maximum smoothing would occur if $\rho = -1$. Previous studies have shown that as the distance between wind plants increases, the correlation between their outputs decreases. The standard deviation of summed time series signals is dependent on the correlation between each individual time series signal (Eq. (4); Giebel, 2000).

$$\sigma_{sum}^2 = \frac{1}{N^2}\sum_i \sum_j \sigma_i \sigma_j corr_{ij} \tag{4}$$

3.5. Step change analysis

The most common time domain method used in wind power studies is a step change analysis (see for example Wan, 2001, 2004) where the change in power for a given time step is calculated and either reported as power (e.g. MW) or as a percentage of the rated capacity of a wind plant (Eq. (5)). We calculate step changes as a percentage of the maximum power produced by a wind plant or summed plants (Eq. (6)).

$$\Delta P = P(t+\tau) - P(t) \text{ or } \Delta P = \frac{P(t+\tau) - P(t)}{P_{Nameplate\ \ capacity}} \times 100 \tag{5}$$

$$\Delta P = \frac{P(t+\tau) - P(t)}{\max(P)} \times 100 \tag{6}$$

We calculate step changes at 30-, 60-min and 1-day time intervals because they are important to ancillary services and day-ahead electricity markets. We plot the maximum step change observed versus the distance from the original starting wind plant to the next wind plant interconnected.

3.6. Frequency domain

To characterize the smoothing of wind power's variability as a function of frequency as wind plants are interconnected, we analyze wind power in the frequency domain. Our results can be used to help determine the most economical generation portfolio to compensate for wind's variability. For the Texas wind plant data, we compute the discrete Fourier transform of the time series of output in order to estimate the power spectrum (sometimes termed the power spectral density or PSD) of the power output of a wind farm.

One of the attributes of power spectrum estimation is that increasing the number of time samples does not decrease the standard deviation of the PSD at any given frequency f_k. In order to take advantage of a large number of data points in a data set to reduce the variance at f_k, the data set may be partitioned into K time segments. The Fourier transform of each segment is taken and a PSD constructed. The PSDs are then averaged at each frequency, reducing the variance of the final estimate by the number of segments (and reducing the standard deviation by $1/\sqrt{K}$). The length of a data set determines the lowest frequency that can be resolved and segmenting increases the lowest frequency we are able to resolve in a signal by a factor of K (Apt, 2007; Press et al., 1992). Since we wish to characterize wind power variability in the time range of current market operations (24 h–15 min), the decreased ability to examine frequencies corresponding to very long times is a small price to pay for the decreased variance.

A Fourier transform requires evenly sampled data points to transform a signal from the time domain to the frequency domain. The Texas wind plant output data are complete for the time period (2008) examined. However, the ASOS data have significant gaps. For example, the longest continuous data segment for one ASOS station was 42 days and the longest coincident continuous data segment of the 40 summed ASOS stations was 12 h. The high percentage of missing data would limit our frequency analysis in two ways. First, we would be able to use only the 12 h of coincident continuous good wind speed data. Second, we would not be able to use segmenting to reduce the variability of the ASOS PSDs because the length of the coincident continuous good data is so short. To overcome the limitations imposed by the high percentage of missing ASOS data we calculate PSDs by using a Lomb periodogram instead of a periodogram estimated using a Fourier transform. The Lomb periodogram (Lomb, 1976) was developed for use in intermittent astrophysics data (Eq. (7)) and does not require evenly sampled data points to calculate the PSD of a signal. Instead of calculating the Fourier frequencies of a signal, it applies a least-squares fit of sinusoids to the data to obtain the frequency components. The time delay component τ in Eq. (7) ensures the frequencies produced by the Lomb periodogram are orthogonal to one another. We implement the Lomb periodogram by using the algorithm of Press et al. (1992).

$$\text{Lomb Periodogram}\quad P_N(\omega) = \frac{1}{2\sigma^2}\left\{\frac{\left[\sum_j (h_j - \bar{h})\cos\omega(t_j - \tau)\right]^2}{\sum_j \cos^2\omega(t_j - \tau)} + \frac{\left[\sum_j (h_j - \bar{h})\sin\omega(t_j - \tau)\right]^2}{\sum_j \sin^2\omega(t_j - \tau)}\right\} \tag{7}$$

Subject to the constraint:

$$\tan(2\omega\tau) = \frac{\sum_j \sin 2\omega t_j}{\sum_j \cos 2\omega t_j}$$

In computing the PSDs, we use 8 segments for the ERCOT data and 32 segments for the ASOS data to reduce the variability of using a year's worth of data. The algorithm used to implement the Lomb periodogram requires two factors, ofac and hifac, to be defined for each signal. The first factor, ofac, is an oversampling factor that we set to 6 for ASOS data and 1 for ERCOT data. The

second factor, hifac, determines the highest frequency the algorithm is able to resolve. We calculate hifac for each signal to produce the correct Nyquist frequency.

Kolmogorov (1941) proposed that the energy contained in turbulent fluids is proportional to the frequency of the turbulent eddies present in the fluid, $E \propto f^{\beta}$, with $\beta = -5/3$. Apt (2007) has shown the power spectrum of a wind plant's power output follows a Kolmogorov spectrum between frequencies of 30 s and 2.6 days. We expect departures from Kolmogorov of $\beta < -5/3$ if any smoothing occurs when wind plants are interconnected. As wind plants are interconnected we estimate β by linearly regressing the log of the PSD of the summed wind power between the frequencies of 1.2×10^{-5} and 5.6×10^{-4} Hz (24 h–30 min).

Kolmogorov's relationship is valid for wind only for frequencies corresponding to times of approximately 24 h or less. It has been shown the spectra of wind speed turbulence flatten for longer frequencies, indicating wind has constant energy in its lower frequencies (longer than a few days) (Jang and Lee, 1998). We use a modified von Karman formulation (Eq. (8)) for wind speed turbulence spectrum to model the power spectrum of one wind plant over the frequency range of 43 days–30 min (Kaimal, 1972).

To estimate the smoothing arising from interconnecting wind plants, we determine if departures from a Kolmogorov spectrum occur in the following manner. We fit Eq. (8) to the PSD of a single wind plant to determine a value for B.

$$PSD(f) = \frac{A}{1 + Bf^{-5/3}} \tag{8}$$

As we add wind plants to the single wind plant, we fit Eq. (8) to the resulting summed PSD to determine a value for A and produce an appropriately scaled single wind plant model PSD. We then compare the slope of the log of the summed PSD to the $-5/3$ slope of the single wind plant model in the Kolmogorov region between frequencies corresponding to 30 min and 24 h. We measure deviations from the spectrum of Eq. (8) by dividing the power contained in each frequency of the summed PSD by the power estimated in each frequency of the single wind plant model. If no smoothing occurs when wind plants are interconnected the result should be close to 1 for all frequencies. If there is a reduction in variability then there will be frequencies for which the fraction is less than 1. Finally, we use a linear regression on the log of the fractions to display the mean fraction response versus frequency.

3.7. Wind drought analysis

Analyzing long-term variations in wind power production is important for system planning. If significant drought periods occur, system planners must ensure adequate resources and renewable energy credits (RECs) are available to cover the wind power underproduction. Similarly, wind production that is significantly above the long-term average may depress the market price for RECs and increase the requirements for compensating power sources.

We use hourly NOAA data to estimate the yearly energy production of wind turbines from 1973 to 2008. We scale the wind speed measurements to 80 m hub heights (see scaling wind data to hub heights section) and transform it to hourly power data with a power curve (see interconnecting wind plants section). A surface roughness of 0.03 m is assumed for all of the airports. For each year the hourly power data from all 16 turbines is summed and compared to the mean yearly power production for the 35-year period.

4. Results

4.1. Frequency domain

In Fig. 3, we show the ERCOT PSD results for 1, 4, and 20 wind plants using 15 min time resolution data for 2008. A single wind plant follows a Kolmogorov spectrum ($f^{-5/3}$) from $1.2-10^{-5}$ to 5.6×10^{-4} Hz (corresponding to times of 24 h–30 min). When 4 wind plants are added together, the power contained in this region decreases with frequency at a faster rate ($f^{-2.49}$ instead of $f^{-1.67}$). For 20 wind plants the power decreases even more rapidly with increasing frequency ($f^{-2.56}$). Adding wind plants together does not appreciably reduce the 24 h peak. BPA's summed wind power ($f^{-2.2}$) shows less smoothing than ERCOT's wind power, very likely because 17 of BPA's 19 wind plants are located within 170 km of each other in the Columbia River gorge and BPA's 19 wind plants are separated by at most 290 km.

The amplitude of variability of 20 interconnected wind plants has ~95% less power at a frequency of 2.8×10^{-4} Hz (corresponding to 1 h) than that of a single wind plant (Fig. 4). The reduction in variability has very rapidly diminishing returns to scale, as interconnecting 4 wind plants gives an 87% reduction in variability at this frequency and interconnecting the remaining 16 wind plants produces the remaining 8% reduction. The maximum reductions in variability occur at the higher frequencies and dimish as the frequency decreases until at 24 h there is no reduction in variability (Fig. 3). Fig. 5 shows the reduction in variability achieved as a function of the number of interconnected wind plants for frequencies corresponding to 1, 6, and 12 h.

We calculate β (f^{β}) for simulations where each of ERCOT's 20 wind plants is used as the starting location and the remaining 19 wind plants are interconnected to it in order of their distance (closest to farthest). We use the resulting 400 data points to model the change in β due to three factors: ρ, the correlation coefficient between the interconnected wind plants and the next wind plant to be interconnected; $P_{Nameplate\ ratio}$, the ratio between the nameplate capacity of the wind plant to be interconnected and the nameplate capacity of the interconnected wind plants; and N, the number of wind plants interconnected. Eq. (9) is the result of linearly regressing the log of the change in β with the three variables (R^2 is 0.77 and all variables are significant to a 99% level).

$$\log \Delta\beta = 7.6\rho + 0.91P_{Nameplate\ ratio} - 0.1N - 8.9 \tag{9}$$

The PSD of 40 interconnected modeled 1.5 MW GE turbines located throughout the Great Plains and Midwest did not depart from a Kolmogorov spectrum. We have eliminated as a possible cause the different time resolutions by averaging the ASOS data at 15 min intervals (the ERCOT sampling rate). It is possible that the discrepancy between the ASOS simulated power output and the observed ERCOT power output spectra may arise from intra-wind-farm aerodynamic effects, but further analysis is required, including the determination of the frequency dependence of the smoothing as a function of wind farm size.

4.2. Generation duration curves

We have computed normalized generation duration curves for a single ERCOT wind plant, 20 interconnected ERCOT wind plants, and BPA's wind power (Fig. 6). Also shown is the average normalized generation duration curve of ERCOT's 20 wind plants interconnected with their nearest three neighbors and the area encompassed by ± 1 standard deviation. One wind plant has a higher probability of achieving close to its nameplate capacity than interconnected wind plants but an increased probability of no wind or low wind power events.

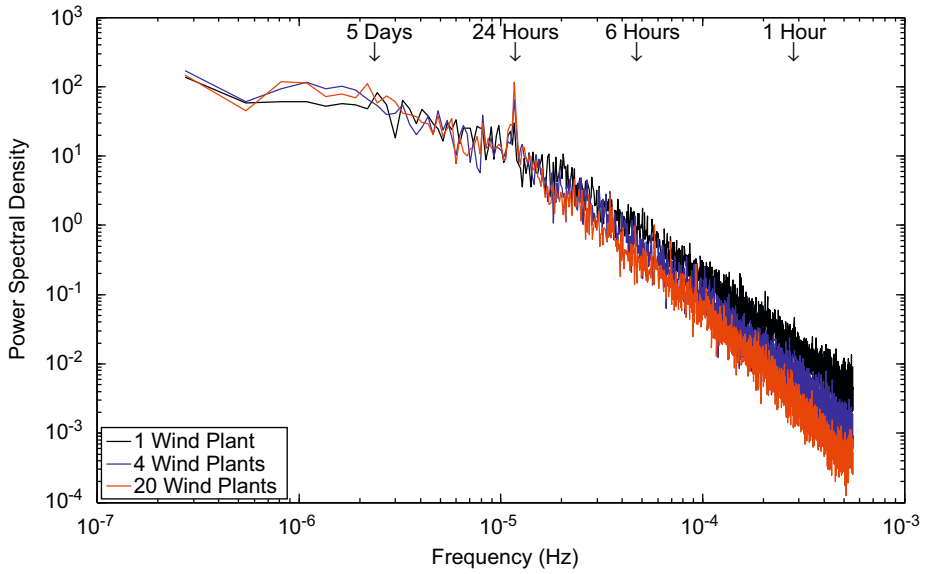

Fig. 3. Power spectral density (with 8 segment averaging, $K=8$) for 1 wind plant, 4 interconnected wind plants, and 20 interconnected wind plants in ERCOT. Wind power variability is reduced as more wind plants are interconnected, with diminishing returns to scale.

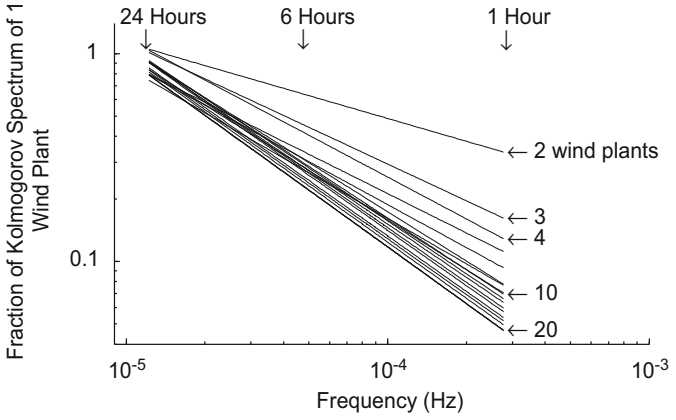

Fig. 4. Fraction of a Kolmogorov spectrum of 1 wind plant for interconnected wind plants over a frequency range of 1.2×10^{-5}–5.6×10^{-4} Hz. As more wind plants are interconnected less power is contained in this frequency range.

Archer and Jacobson (2007) concluded on the basis of meteorological data that interconnected wind plants spread throughout Texas, Oklahoma, Kansas, and New Mexico would produce at least 21% of their rated capacity 79% of the time and 11% of their rated capacity 92% of the time. The ERCOT and BPA data from operating wind turbines do not support that conclusion. ERCOT's 20 interconnected wind plants produced at least 10% of their rated power capacity 79% of the time and at least 3% of their rated capacity 92% of the time. BPA's 19 interconnected wind plants produced at least 3% of their rated capacity 79% of the time and 0.5% of their rated capacity 92% of the time. Hereinafter we define "firm power" for a generator as an availability range of 79–92%.

Archer and Jacobson's (2007) simulations produce baseload capacity equivalents for wind power that are 2–20 times greater than those observed in the ERCOT and BPA data. Two effects may be responsible for the discrepancy between our results and Archer and Jacobson's results. The first is that Archer and Jacobson analyze a larger geographical area than the encompassed by ERCOT or BPA. The second is Archer and Jacobson use individual model wind turbines while we use data from operating wind plants.

The average generation duration curve of four interconnected ERCOT wind plants shows that a small number of interconnected wind plants achieves the majority of the smoothing of wind power's variability and corresponds to the result obtained from our power spectral density analysis. 19 BPA and 20 ERCOT interconnected wind plants similarly achieve only 70–88% of their nameplate capacities but BPA's wind power has a higher probability of low to no wind power occurances. The higher probability of low to no wind events in BPA's system is likely because of the limited geographic dispersion of BPA's wind plants noted in the preceding section.

4.3. Pairwise correlations of wind power output

In Fig. 7 we show the correlation coefficients between pairs of wind plants versus the geographical distance between the wind plants, using measured 15-min wind power averages from 20 wind plants in Texas for 2008. Wind plants that are located less than 50 km apart tend to have highly correlated power outputs ($0.7<\rho<0.9$), while wind plants located more than 500 km apart show lower correlation ($\rho<0.3$). All of the correlation coefficients were greater than zero at the 99% significance level (t-test).

The exponential fit shown in Fig. 7, $\rho\propto\exp(-distance/D)$, has a decay parameter D of 305 km and an intercept of $\rho=0.89$ at zero separation distance. A linear regression of log-transformed correlation coefficients against distance has an R^2 of 0.55 (i.e. the exponential model explains about half of the variation in the correlation coefficients).

Eight pairs of wind plants, between 200 and 300 km apart, have correlation coefficients lower than 0.2 that lie below the overall trend. These eight pairs are Delaware Mountain and Kunitz paired with each of Woodward Mountain, Indian Mesa, Southwest Mesa, and King Mountain (Table A2 in the Appendix). This may reflect the influence of local topography and climate patterns and demonstrates that geographical proximity does not necessarily imply high correlation. Removing these eight points increases D to 320 km; the difference between this value and that of the full data set is not statistically significant (t-test, 95% significance level), so the cluster of 8 points does not exert strong leverage on the model.

Giebel (2000) performed a similar analysis for wind power in Europe and found D to be 641 km (green line in Fig. 7). While the current study analyzes 15-min wind energy data sampled

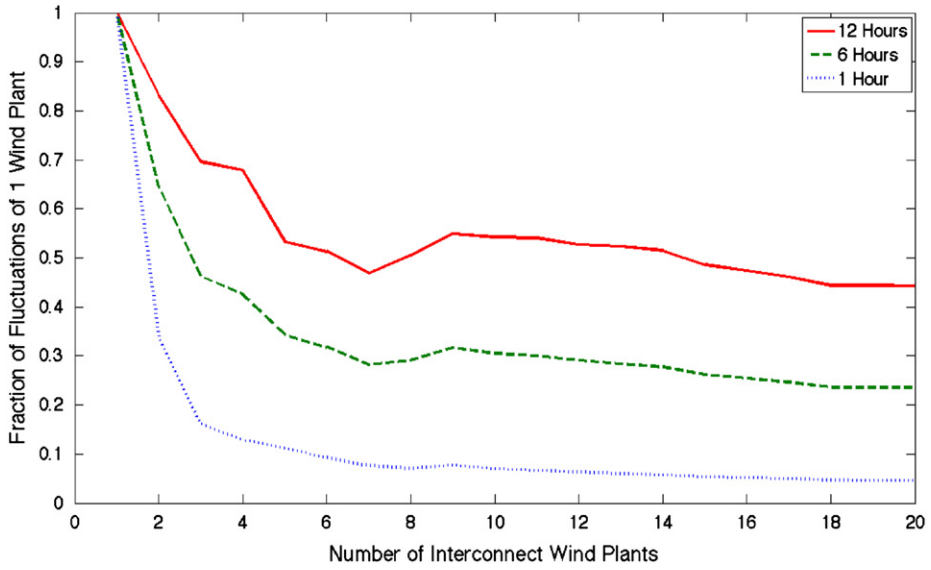

Fig. 5. Fraction of a Kolmogorov spectrum of different time scales versus the number of interconnected wind plants. Interconnecting 4 or 5 wind plants achieves the majority of the reduction of wind power's variability. We note that reductions in wind power variability are dependent on more than just the number of wind plants interconnected (e.g. size, location, and the order in which the wind plants are connected; see Eq. 9).

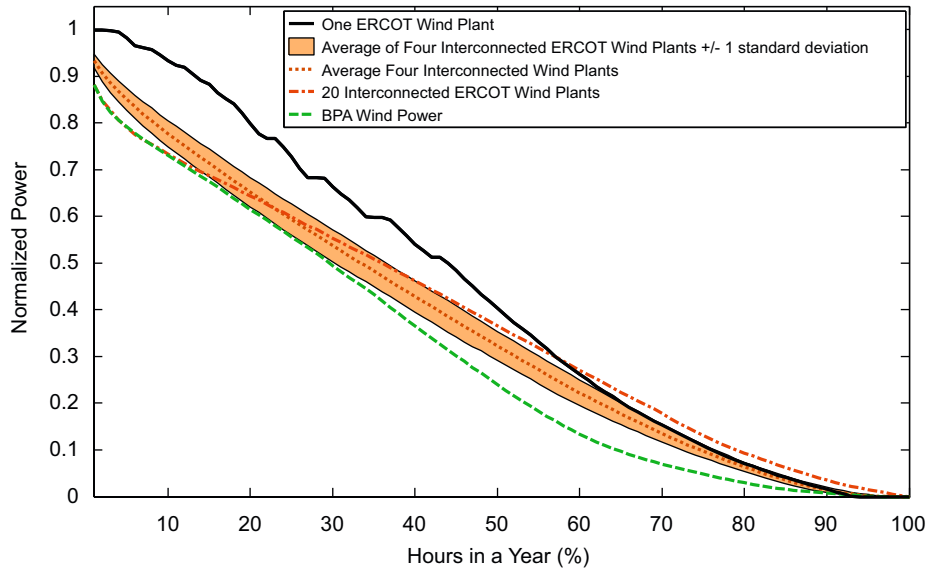

Fig. 6. Normalized generation duration curves for ERCOT interconnected wind plants and BPA's total wind power for 2008. The average normalized generation duration curve of ERCOT's 20 wind plants interconnected with their nearest 3 neighbors is plotted (dotted line) with the area encompassed by one standard deviation (tan area).

constantly for 2008, Giebel (2000) acquired data by applying a power curve to 10-min wind speed averages sampled every 3 h, thus obtaining 10-min wind power averages at 3-h intervals. To assess the distortion in cross-correlations that this difference introduces, 1 week of 10-s wind power data for two wind plants in Texas and Oklahoma was processed to mimic Giebel's data as well as that of the current study. The correlation coefficient for 10-min averages taken every 3 h was 0.31, and for consecutive 15-min averages was also 0.31. The proximity of these values suggests that the difference in data sampling frequencies between the current study and Giebel (2000) does not introduce distortions that prohibit comparison.

Fixing the best-fit intercept for the Texas data in Fig. 7, the decay parameter of the European model (641 km) differs from that of the best-fit Texas model (305 km) at the 99% significance level (t-test). The R^2 of Giebel's model applied to the Texas data is 0.05, which reflects the poor fit of the European model to the Texas data.

A significantly higher decay parameter for wind power in Texas would imply that more smoothing occurs over a given distance in Texas than in Europe; however, large variation in correlation coefficients for the European data prohibits a firm comparison. European wind speed cross-correlation data for December 1990–1991 has an exponential best-fit with $D=723$ km (Giebel, 2000). The correlation coefficients show a large degree of scatter, especially in the 0–500 km region that overlaps with the data of the current study; between 400 and 500 km, ρ for the European wind speed data ranges from approximately 0.1–0.7, while ρ for the Texas wind power data ranges from 0.1 to 0.3. Assuming a similar degree of scatter in ρ for the resulting European wind power time series, no significant difference between cross-correlations of Texas and European wind power data can be determined by comparing the current study and Giebel (2000); the European exponential model is a poor fit for the Texas data, but the Texas model could fit the European data

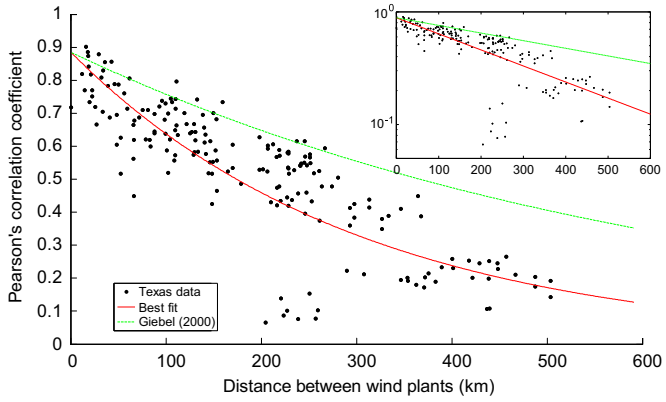

Fig. 7. Correlation coefficients vs. distance between pairs of wind plants (inset shows the data on a semi-log plot).

comparably to the best-fit model of Giebel (2000), especially at distances below 500 km.

4.4. Step change analysis

Fig. 8 shows the maximum ASOS 30-, 60-min and 1-day percent step changes in power as a function of distance when KCNK (Concordia, Kansas), a station close to the geographic centroid of the ASOS airports, is used as the starting station, and additional stations are added based on their distance from the starting station. Fig. 9 is constructed using KMOT (Minot, North Dakota), the station farthest from the geographical center of mass, as the starting station.

Adding together wind plants reduces the substantial step changes in power experienced by individual wind plants. As more distant wind plants are interconnected, the maximum step

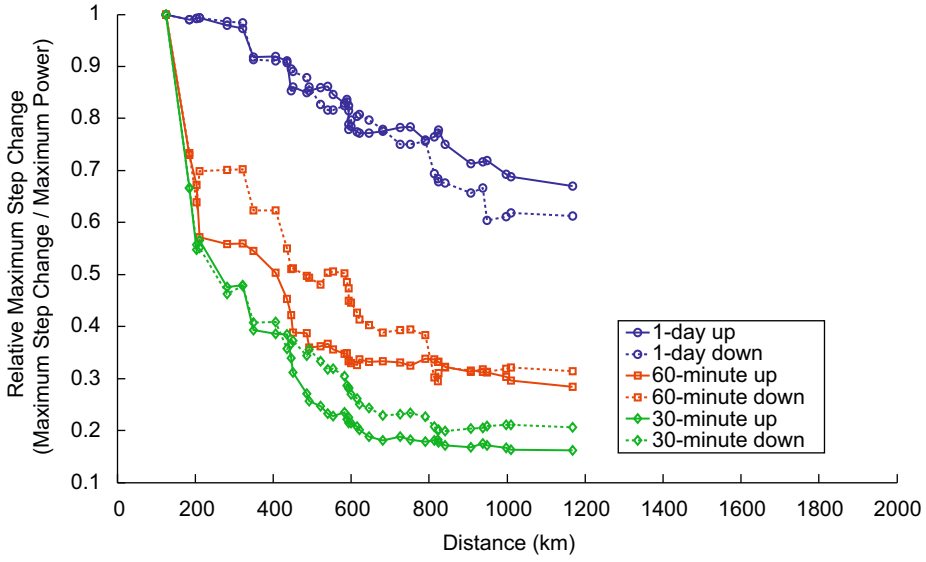

Fig. 8. ASOS step change analysis using KCNK (Concordia, Kansas) as the starting location. Each point represents an additional interconnected station. The relative maximum step change, measured as the maximum step change divided by the maximum power, decreases with distance as more wind plants are interconnected.

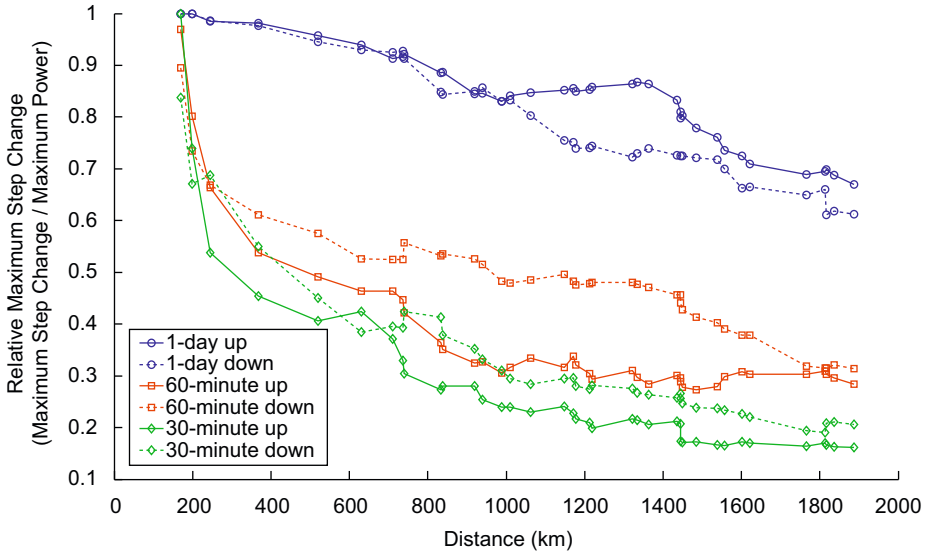

Fig. 9. ASOS step change analysis using KMOT (Minot, North Dakota) as the starting location. Each point represents an additional interconnected station. The relative maximum step change, measured as the maximum step change divided by the maximum power, decreases with distance as more wind plants are interconnected.

change in power relative to the maximum power produced reaches an asymptote of 15–30% for step changes of an hour or less. The reductions in variability are approximately equal to those observed by Milborrow (2001) (a maximum hourly step change of 18%) and are less than what BPA experienced in 2008 (a maximum hourly step change of 63%). BPA's control area is significantly smaller than the geographic region spanned by the 40 ASOS sites. The largest 30-min increase or decrease in power estimated from 40 interconnected ASOS wind plants was 15% of the maximum wind power produced. The maximum 1-day step changes are also reduced as more distant wind plants are interconnected although a reduction of at most 20% is achieved.

The reductions are obtained over relatively short distances with ~50% of the reductions occurring within 400 km. In Fig. 8, 93% of the reductions occur in the first 600 km and 7% occurs between distances of 600 and 1200 km. If the reference wind plant is at a geographic extreme rather than the centroid (Fig. 9), 93% of the reductions occur in the first 1000 km.

Fig. 10 shows the maximum ERCOT 30-, 60-min, and 1-day percent step changes in power when ERCOT wind plant 1 (Delaware Mountain), the wind plant farthest from the geographic centroid of ERCOT's wind plants, is used as the starting wind plant. Similar reductions in variability to those simulated from ASOS data are produced when ERCOT wind plants are interconnected. Reductions of 42% for 30-min step changes, 50% for 60-min step changes, and 16% for 1-day step changes are achieved when wind plants within 500 km are interconnected. The reductions for ERCOT are observed over shorter distances than predicted by the ASOS results. In ERCOT's system, wind power ramps up faster than it ramps down for each of the step change intervals analyzed. If system operators are to match wind's fluctuations exactly, they will need to have a larger capacity from generators and demand response to ramp down their power than they will require from them to ramp up.

4.5. Are there wind droughts?

We estimated yearly variation in wind energy production from modeled 1.5 MW turbines at 16 locations over the years 1973–2008 (Fig. 11). Also plotted is the annual energy produced from hydroelectric power in the United States for the same time span. We normalized each of the results by their mean. The standard deviation for the estimated wind production was 6% of the mean energy produced per year. The largest deviation from the mean occurred in 1988 when the estimated wind energy production was 14% more than the mean annual production. The largest negative deviation from the mean occurred in 1998 when estimated wind energy produced was 10% less than the mean annual production. The standard deviation for the actual hydroelectric production was 12% of the mean energy produced per year for the 36-year period. US hydropower's largest positive deviation from the mean occurred in 1997 when hydropower production was 26% above the mean. The largest negative deviation occurred in 2001 when hydropower production was 23% below average.

Thus, yearly wind energy production from the sample of 16 airports in the central and southern Great Plains is predicted to exhibit long-term variations, and these are about half that observed nationally for hydropower (we note that the bulk of hydropower production is regionally concentrated).

5. Analysis

The variability of interconnected wind plants is less than that of individual wind plants when measured in the time domain with step

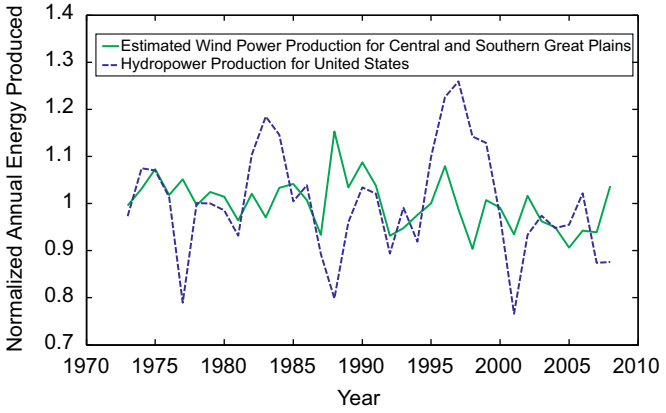

Fig. 11. Normalized predicted annual wind energy production from 16 wind turbines located throughout the Central and Southern Great Plains. The normalized annual hydropower production for the United States is also plotted for comparison.

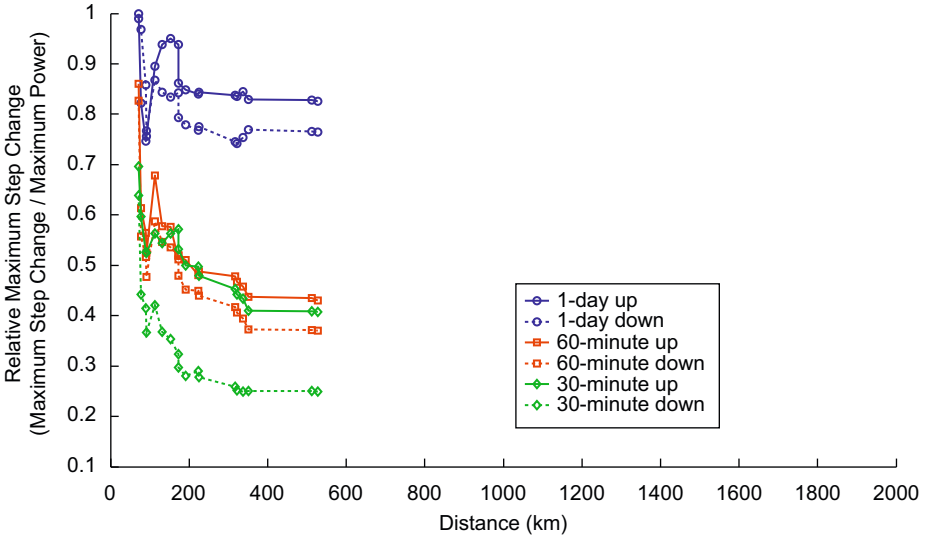

Fig. 10. ERCOT step change analysis when wind plant 1 (Delaware Mountain, TX) is used as the starting location. The relative maximum step change, measured as the maximum step change divided by the maximum power, decreases with distance as more wind plants are interconnected.

change analyses and in the frequency domain with power spectrum analyses. The amount of smoothing is a predictable function of frequency, correlation coefficient, nameplate capacity ratio, and the number of interconnected wind plants. Reductions in variability diminish as more wind plants are interconnected. Finally, yearly wind power production is likely to vary, and have year-to-year variations about half that observed nationally for hydropower.

These results do not indicate that wind power can provide substantial baseload power simply through interconnecting wind plants. ERCOT's generation duration curve shows wind power reliably provides 3–10% of installed capacity as firm power (as defined above) while BPA's generation duration curve shows 0.5–3% of their wind power is firm power. The frequency domain analyses have shown that the power of interconnected wind plants will vary significantly from day to day and the results of the step change analyses show day-to-day fluctuations can be 75–85% of the maximum power produced by a wind plant (Figs. 8–10).

The benefit of interconnecting wind plants is a significant reduction in the high-frequency variability of wind power. Reductions in the relative magnitude of the 30-min and hourly step changes will reduce the per MWh ancillary service costs of wind energy. The reductions will also improve the root mean-square error of wind energy forecasts for a system's total wind energy production but not the forecast error for individual wind plants. Estimating the value of these benefits is difficult due to the proprietary algorithms used by system operators. We have provided system planners with a metric that better characterizes the variability of large penetrations of wind power. System planners can then identify the resources needed to compensate the variability and calculate the associated costs.

Acknowledgments

The authors thank Jack Ellis, Lester B. Lave, Ralph Masiello, Gregory Reed, Steve Rose, and Mitchell Small for useful comments and conversations. This work was supported in part by a grant from the Alfred P. Sloan Foundation and EPRI to the Carnegie Mellon Electricity Industry Center, by the US National Science Foundation under NSF Cooperative Agreement No. SES-0345798, and by the Doris Duke Charitable Foundation, the Department of Energy National Energy Technology Laboratory, and the Heinz Endowments for support of the RenewElec program at Carnegie Mellon University.

Appendix

Tables A1 lists the airport sites from which ASOS wind speed data were obtained. Tables A2 lists the ERCOT wind plants from which wind power data were obtained.

Table A1
Table of ASOS stations used to obtain wind speed data.

Station	State	Latitude			Longitude			Hourly data used?
		Degrees	Minutes	Seconds	Degrees	Minutes	Seconds	
KEST	IA	43	24	29.73	94	44	47.94	
KSPW	IA	43	9	57.64	95	12	20.15	
KMCW	IA	43	9	34.76	93	20	12.56	Yes
KAMW	IA	41	59	59.49	93	37	16.3	
KALO	IA	42	33	22.35	92	23	47.19	
KDDC	KS	37	46	0.28	99	57	58.68	Yes
KGCK	KS	37	55	43.6	100	43	32.48	
KCNK	KS	39	32	57	97	39	8	Yes
KRSL	KS	38	52	16.67	98	48	31.04	
KAAO	KS	37	44	51.3	97	13	16	
KEMP	KS	38	19	55.34	96	11	18.26	
KGLD	KS	39	22	17.239	101	41	56.371	Yes
KICT	KS	37	38	59.8	97	25	59	Yes
KRWF	MN	44	32	48.41	95	5	0.09	
KRST	MN	43	54	31.73	92	29	48.18	Yes
KFCM	MN	44	49	42.71	93	27	37.5	
KAXN	MN	45	51	56.85	95	23	32.27	Yes
KBIS	ND	46	46	23.07	100	44	58.21	Yes
KJMS	ND	46	55	44.34	98	40	41.91	
KDIK	ND	46	47	46.94	102	48	1.33	Yes
KMOT	ND	48	15	33.78	101	16	51.9	Yes
KFAR	ND	46	55	17.62	96	48	49.63	Yes
KCAO	NM	36	26	43.89	103	9	14.13	
KLVS	NM	35	39	15.2	105	8	32.6	
KCSM	OK	35	20	26.74	99	11	55.82	
KFDR	OK	34	21	7.5449	98	59	2.0727	
KGAG	OK	36	17	43.94	99	46	35.125	
KHBR	OK	34	59	28.7	99	3	5	
KPWA	OK	35	32	3	97	38	49	
KOKC	OK	35	23	35.12	97	36	2.64	Yes
KABI	TX	32	24	23.49	99	41	0.66	Yes
KAMA	TX	35	13	8.52	101	42	18.84	Yes
KCDS	TX	34	25	58.79	100	17	35.28	
KDHT	TX	36	1	20.41	102	32	58	
KGDP	TX	31	42	3.6	106	16	34.36	
KLBB	TX	33	39	48.86	101	49	22.18	Yes
KMAF	TX	31	56	42.98	102	12	15.65	Yes
KODO	TX	31	55	18.52	102	23	10.74	
KINK	TX	31	46	46.69	103	12	10.28	
KSPS	TX	33	59	19.666	98	29	30.816	

Table A2
ERCOT wind plants.

Number	Name	Latitude	Longitude
1	Delaware Mountain	31.6486	−104.75
2	Woodward	30.9575	−102.377
3	Indian Mesa	30.9333	−102.182
4	Southwest Mesa	31.0844	−102.108
5	King Mountain	31.2213	−102.161
6	Kunitz	31.3478	−104.4723
7	Capricorn Ridge	31.8207	−100.793
8	Airtricity	32.0649	−101.536
9	Sweetwater	32.32	−100.4
10	Trent Mesa	32.429	−100.199
11	Buffalo Gap	32.2287	−100.062
12	Horse Hollow	32.344	−99.9853
13	Callahan Divide	32.299	−99.872
14	Post Oak	32.7234	−99.2963
15	Mesquite	32.7234	−99.2963
16	Camp Springs	32.7556	−100.698
17	ENA Snyder	32.7921	−100.918
18	Brazos	32.9574	−101.128
19	Red Canyon	32.9389	−101.316
20	Whirlwind	34.0862	−101.086

References

Apt, J., 2007. The spectrum of power from wind turbines. Journal of Power Sources 169, 369–374.

Archer, C.L., Jacobson, M.Z., 2007. Supplying baseload power and reducing transmission requirements by interconnecting wind plants. Journal of Applied Meteorology and Climatology 46, 1701–1717.

BPA, 2009. BPA announces rate changes. Bonneville Power Authority, News Releases, PR 31 09. Available at: 〈http://www.piersystem.com/go/doc/1582/292435/〉.

CAISO, 2007. Draft: integration of renewable resources report. California Independent System Operator, Renewables Workgroup. Available at: 〈http://www.caiso.com/1c60/1c609a081e8a0.pdf〉.

Cha, P., Molinder, J., 2006. Fundamentals of Signals and Systems: A Building Block Approach.. Cambridge, New York.

Czisch, G., Ernst, B., 2001. High wind power penetration by the systematic use of smoothing effects within huge catchment areas shown in a European example, Windpower 2001. American Wind Energy Association, Washington, DC 2001. Available at:〈http://www.iset.uni-kassel.de/abt/FB-I/projekte/awea_2001_czisch_ernst.pdf〉.

Dobesova, K., Apt, J., Lave, L.B., 2005. Are renewables portfolio standards cost-effective emission abatement policy? Environmental Science & Technology 39 (22) 8578–8583.

DOE, 2008. 20% Wind Energy by 2030. US Department of Energy, Office of Energy Efficiency and Renewable Energy. Available at: 〈http://www1.eere.energy.gov/windandhydro/pdfs/41869.pdf〉.

DSIRE. Database of State Incentives for Renewables and Efficiency, 2009. www.dsireusa.org.

EIA, 2009. Annual Energy Review—Table 8.2a Electricity Net Generation: Total (All Sectors), 1949–2008. US Energy Information Agency. Available at: 〈http://www.eia.doe.gov/emeu/aer/txt/stb0802a.xls〉.

EnerNex, 2006. 2006 Minnesota Wind Integration Study, Volume 1. EnerNex Corporation. Available at: 〈http://www.uwig.org/windrpt_vol%201.pdf〉.

GE, 2008. ERCOT wind impact\integration analysis. General Electric. Available at: 〈http://www.ercot.com/meetings/ros/keydocs/2008/0227/ERCOT_final_pres_d1_w-o_backup.pdf〉.

Giebel, G., 2000. On the benefits of distributed generation of wind energy in Europe. Ph.D. Dissertation, Carl von Ossietzky University of Oldenburg, 2000, 104 pp. Available at: 〈http://www.drgiebel.de/GGiebel_DistributedWindEnergyInEurope.pdf〉.

Hirst, E., 2002. Integrating wind energy with the BPA power system: preliminary study. Bonneville Power Authority. Available at: 〈http://www.bpa.gov/Power/pgc/wind/Wind_Integration_Study_09-2002.pdf〉.

International Energy Agency, 2005. Variability of Wind Power and Other Renewables—Management Options and Strategies. Available at: 〈http://www.iea.org/papers/2005/variability.pdf〉.

Jang, J., Lee, Y., 1998. A study of along wind speed power spectrum for Taiwan area. Journal of Marine Science and Technology 6.1, 71–77.

Kahn, E., 1979. The reliability of distributed wind generation. Electric Power Systems Research 2, 1–14.

Kaimal, J.C., 1972. Spectral characteristics of surface layer turbulence. Journal of the Royal Meteorological Society 98, 563–589.

Kolmogorov, A., 1941. The local structure of turbulence in incompressible viscous fluids at very large Reynolds numbers. Dokl. Akad. Nauk. SSSR, 30, 301–305. Reprinted (1991) Royal Society of London. Proceedings: Mathematical and Physical Sciences 434, 9–13.

Lomb, N.R., 1976. Least-squares frequency analysis of unevenly spaced data. Astrophysics and Space Science 39, 447–462.

Milborrow, D., 2001. Penalties for intermittent sources of energy. Working Paper for UK Cabinet Performance and Innovation Unit (PIU) Energy Review. Available at: 〈http://www.cabinetoffice.gov.uk/media/cabinetoffice/strategy/assets/milborrow.pdf〉.

Milligan, M., Porter, K., 2005. Determining the capacity value of wind: a survey of methods and implementation. "Windpower 2005" American Wind Energy Association, Denver, 2005, National Renewable Energy Laboratory, Conference Paper, NREL/CP-500-38062. Available at: 〈http://www.nrel.gov/docs/fy05osti/38062.pdf〉.

National Oceanic and Atmospheric Administration, Department of Defense, Federal Aviation Administration, United States Navy, 1998. Automated Surface Observing System (ASOS) User's Guide. Available at: 〈http://www.nws.noaa.gov/asos/pdfs/aum-toc.pdf〉.

Over, T.M., D'Odorico, P., 2002. Scaling of surface wind speed. In: Lee, Jeffrey A., Zobeck, Ted M. (Eds.), Proceedings of ICAR5/GCTE-SEN Joint Conference, International Center for Arid and Semiarid Lands Studies, Texas Tech University, Lubbock, TX, USA, Publication 02-2, p. 50. Available at: 〈http://www.csrl.ars.usda.gov/wewc/icarv/15a.pdf〉.

Press, W.H., Teukolsky, S.A., Vetterling, W.T., Flannery, B.P., 1992. Numerical Recipes in FORTRAN: The Art of Scientific Computing second ed. Cambridge University Press, Cambridge.

Seinfeld, J.H., Pandis, S.N., 2006. Atmospheric Chemistry and Physics: From Air Pollution to Climate Change second ed. Wiley, Hoboken.

Vincenty, T., 1975. Direct and inverse solutions of geodesics on the ellipsoid with application of nested equations. Survey Review 23, 88–93.

Wan, Y., 2001. Wind Power Plant Monitoring Project Annual Report. National Renewable Energy Laboratory, Technical Report, NREL/TP-500-30032. Available at: 〈http://www.nrel.gov/docs/fy01osti/30032.pdf〉.

Wan, Y., 2004. Wind power plant behaviors: analyses of long-term wind power data. National Renewables Energy Laboratory, Technical Report, NREL/TP-500-36551. Available at: 〈http://www.nrel.gov/docs/fy04osti/36551.pdf〉.

Waxman, H., Markey, E., 2009. H.R. 2454: American clean energy and security act of 2009. United States House of Representatives, 111th Congress. Available at: 〈http://www.govtrack.us/data/us/bills.text/111/h/h2454pcs.pdf〉.